Article

Katanin Severing and Binding Microtubules Are Inhibited by Tubulin Carboxy Tails

Megan E. Bailey,[1,2] Dan L. Sackett,[3] and Jennifer L. Ross[2,*]

[1]Molecular and Cellular Biology Graduate Program and [2]Department of Physics, University of Massachusetts-Amherst, Amherst, Massachusetts; and [3]Program in Physical Biology, Eunice Kennedy Shriver National Institute of Child Health and Human Development, National Institutes of Health, Bethesda, Maryland

ABSTRACT   Microtubule dynamics in cells are regulated by associated proteins that can be either stabilizers or destabilizers. A class of destabilizers that is important in a large number of cellular activities is the microtubule-severing enzymes, yet little is known about how they function. Katanin p60 was the first ATPase associated with microtubule severing. Here, we investigate the activity of katanin severing using a GFP-labeled human version. We quantify the effect of katanin concentration on katanin binding and severing activity. We find that free tubulin can inhibit severing activity by interfering with katanin binding to microtubules. The inhibition is mediated by the sequence of the tubulin and specifically depends on the carboxy-terminal tails. We directly investigate the inhibition effect of tubulin carboxy-terminal tails using peptide sequences of α-, β-, or detyrosinated α-tubulin tails that have been covalently linked to bovine serum albumin. Our results show that β-tubulin tails are the most effective at inhibiting severing, and that detyrosinated α-tubulin tails are the least effective. These results are distinct from those for other severing enzymes and suggest a scheme for regulation of katanin activity in cells dependent on free tubulin concentration and the modification state of the tubulin.

INTRODUCTION

Microtubules are essential, rigid biopolymers that form part of the cytoskeleton used to support and organize the interior of cells. Along with their associated proteins and enzymes, microtubules are essential for a variety of processes including mitosis, cell migration, and intracellular transport. Since microtubules are involved in diverse processes, it is important for them to dynamically organize and rearrange based on the state of the cell. It has long been known that microtubules have intrinsic dynamics, termed dynamic instability, wherein the filaments grow and shrink stochastically (1). Microtubules will undergo dynamic instability spontaneously in vitro, and microtubule-associated proteins (MAPs) have been shown to modify the dynamics to regulate how these cytoskeletal filaments are remodeled. It is assumed that alteration of microtubule dynamics by MAPs allows for better spatial and temporal control of the microtubule cytoskeleton in the cell.

There are a plethora of MAPs in the cell, including MAPs that stabilize microtubules, aiding in nucleation of filaments and allowing microtubules to grow, and destabilizing MAPs that depolymerize microtubules, cause more frequent catastrophes, or even sever microtubules. The family of enzymatic MAPs that sever microtubules is called microtubule-severing enzymes. Microtubule-severing enzymes are from the enzyme family of ATPases associated with various cellular activites (AAA+) that hexamerize and utilize ATP to perform their functions (2). Microtubule-severing enzymes use their catalytic activity to dismantle microtubules both in vitro and in vivo (3,4). Within the family of microtubule-severing enzymes, there are three known members: katanin, spastin, and fidgetin.

Katanin was the first discovered microtubule-severing enzyme, and it is unique, because it is composed of a 60 kD catalytic subunit, p60, and an 80 kD regulatory subunit, p80 (3,5). Katanin has been shown to be crucial for a variety of functions in several different types of cells. For instance, katanin was discovered as a component of a *Xenopus* mitotic egg extract that caused the destruction of Taxol-stabilized microtubules (6) and later was purified from sea urchin embryos and identified (5). It has been shown to have roles in mitotic cell division, localizing to kinetochore microtubules during metaphase to regulate spindle flux and to shorten microtubules during anaphase A (7). Katanin-p80 works as a regulatory protein that targets p60 to the centrosomes via the WD40 domains in the N-terminal region (3,8). In egg extracts, katanin controls the spindle length in *Xenopus tropicalis* and *X. laevis*, which in some species can be regulated by N-terminal phosphorylation (9,10). Katanin has also been shown to be involved in regulating microtubule length and releasing microtubules from centrosomes in neurons for proper neuronal development to occur (11). Katanin mutants are responsible for fragile plant defects affecting the pattern of deposition of cell-wall materials (12,13), loss of motile function of cilia

Editor: E. Michael Ostap.

in ciliary diseases (14,15), and longer-than-normal meiotic spindles in *Caenorhabdidtis elegans* meiosis, which eventually lose their biorientation (16,17). Recently, we have shown that katanin regulates microtubule length at the cortex of S2 cells and affects cell migration (18).

Despite its having been discovered almost 25 years ago, there are many open questions about katanin's biochemical and biophysical mechanisms. Katanin is an ATPase that has been reported to be stimulated by the presence of the microtubule substrate, requires ATP to oligomerize, and is inhibited by high concentrations of microtubules (tubulin in polymerized form) (3,5,19). The part of tubulin required for severing is the carboxy-terminal tail (CTT); katanin is unable to sever microtubules lacking the CTT (5,20). Structural studies have shown that katanin requires ATP to oligomerize (4). In vitro work combined with modeling has shown indirectly and directly that katanin targets to microtubule defects (21,22).

Much of our understanding of katanin is based on information we know about the other severing enzymes. Both spastin and katanin require ATP and the CTT to function (20,23,24). It has also been shown that spastin severing is inhibited by CTTs and that all three pore loops in spastin's AAA domain are crucial for severing activity (24,25). Based on the crystal structure of spastin, a model of how it severs was proposed. In the presence of ATP, the severing enzyme docks on the microtubule using the N-terminal microtubule-binding domains. The monomers form a hexameric ring, but it is unclear whether this occurs before or after docking on the microtubule. The center of the ring forms a pore with three pore loops that are thought to interact with the CTTs of tubulin and tug the tails to unfold the tubulin and ultimately cause microtubule breakdown (24). Recent work on spastin has begun to dissect the ATPase cycle and precisely pinpoint how many subunits are required to have ATP to sustain severing (20,26). Despite the mechanistic details that have been uncovered, very little is known about how severing enzymes interact with other individual MAPs, or even with tubulin itself.

In the following studies, we use a purified green-fluorescent-protein (GFP)-labeled human version of katanin p60 to perform quantitative measurements of katanin binding and severing activity on microtubules. We find that dimeric tubulin is a potent inhibitor of katanin severing activity; even low levels of free tubulin can inhibit katanin-based severing of Taxol-stabilized microtubules. Performing direct imaging of GFP-Hu-p60 binding, we show that the free tubulin competes with the microtubule filament for binding and that even the CTTs can effectively compete for binding to cause severing inhibition. Using bovine serum albumin (BSA)-CTT chimeric constructs, we show that different isoforms of tubulin are more or less potent at inhibiting severing, with β-tubulin CTTs being the most inhibitory and detyrosinated α-tubulin CTTs being the least inhibitory. Our studies shed new light on a possible inhibitory feedback mechanism of katanin that might function in the cell to shut down katanin activity so that it does not destroy all the microtubules of the cell.

MATERIALS AND METHODS

Protein purification

Unless otherwise stated, chemicals were purchased from Sigma-Aldrich (St. Louis, MO). We received the pMAL-c5x-*X*. laevis p60 from the Heald Lab, and it was purified as previously described (9). We also made an optimized human p60 construct with a maltose binding protein and GFP (GeneWiz, Cambridge, MA). We will refer to the *Xenopus* construct as Xl-p60 and the human construct as GFP-Hu-p60. An isopropyl β-D-1 thiogalactopyranoside-inducible expression system was used for expression and purification. The plasmid was transformed into BL21 competent *Escherichia coli* (New England BioLabs, Ipswich, MA). A lysogeny broth starter culture was grown overnight and added to a 500 mL culture the next day. This culture was grown at 37°C until it reached an OD of 0.8 and then it was induced with 1 mM isopropyl β-D-1 thiogalactopyranoside. The culture was allowed to continue to grow at 16°C for 16 h. The cells were lysed in resuspension buffer (20 mM HEPES-HCl, pH 7.7, 250 mM NaCl, 0.5 mM β-mercaptoethanol, 10% glycerol, and 0.25 mM ATP) via sonication. The lysate was incubated with amylose resin (New England BioLabs) for 1–2 h. The lysate/resin mixture was added to the column and allowed to enter the column completely. Once excess lysate had passed through the column, the column was washed twice with 20 mL of resuspension buffer (20 mM HEPES-HCl, pH 7.7, 250 mM NaCl, 0.5 mM β-mercaptoethanol, 10% glycerol, and 0.25 mM ATP). Then the protein was eluted in elution buffer (20 mM HEPES-HCl, pH 7.7, 250 mM NaCl, 0.5 mM β-mercaptoethanol, 10% glycerol, 0.25 mM ATP, and 10 mM maltose). The approximate concentration was determined using a Bradford assay.

Taxol-stabilized microtubule polymerization

Taxol-stabilized microtubules were made by combining a 1:3–1:20 ratio of labeled rhodamine tubulin (Cytoskeleton, Denver, CO) or homemade Dylight 649 (Thermo Scientific, Waltham, MA) tubulin. The unlabeled tubulin was purified from porcine brains using the method described in (27). Both the unlabeled and labeled tubulins were resuspended in PEM-100 (100 mM K-PIPES, pH 6.8, 2 mM MgSO$_4$, and 2 mM EGTA) to a concentration of 5 mg/mL. Both were incubated on ice for 10 min. The labeled and unlabeled tubulin were combined and spun at 366,000 × g at 4°C for 10 min. To polymerize the microtubules, 1 mM GTP was added to the tubulin and incubated at 37°C for 20 min. To further stabilize the microtubules, 50 μM Taxol was added and they were incubated for 20 min at 37°C. The microtubules were centrifuged at 16,200 × g at 27°C for 10 min. The pellet was resuspended in PEM-100 and 50 μM Taxol.

Denatured tubulin

Denatured tubulin was made by adding 1 M HCl to the tubulin. The tubulin was brought back up to pH 6.8 using KOH.

Subtilisin-treated denatured tubulin

Subtilisin-treated denatured tubulin was made from Taxol-stabilized microtubules that were polymerized by the same procedure as above with several additional steps. After the microtubules were polymerized, they were incubated with 100 μg/mL subtilisin for 45 min. The reaction was stopped with 2 mM PMSF. The microtubules were centrifuged at 16,200 × g at 27°C for 30 min, and the pellet was resuspended in PEM-100 and 1 mM GTP. The

subtilisin-treated microtubules were denatured by adding 1 M HCl. The tubulin was brought back up to pH 6.8 using KOH.

CTT peptide and BSA-CTT chimeras

Chimeric protein constructs of BSA and tubulin CTT peptides were produced using chemical linkage via aromatic-hydrazine-aromatic-aldehyde click chemistry (28). Peptides corresponding to the CTT sequences of human β-tubulin (TUBB, NP_821133; -ATAEEEEDFGEEAEEEA), human α-tubulin (TUBA1A, NP_001257328; -DSVEGEGEEEGEEY), and detyrosinated α-tubulin (-DSVEGEGEGEEEGEE) were obtained from Peptide 2.0 (Chantilly, VA). Tails were used alone, or covalently attached to BSA. BSA was randomly labeled with 1.5 molar excess of succinimidyl 4-formylbenzoate (Solulink, San Diego, CA), and peptides were specifically tagged at their amino termini by reaction with a 3 molar excess of succinimidyl 6-hydrazinonicotinate acetone hydrazone (Solulink). After chromatographic cleanup, the tagged BSA and tagged peptides were allowed to react overnight, followed by removal of the unreacted peptide. The concentration of the recovered BSA and the concentration of the attached CTT peptides were determined by ultraviolet spectroscopy. The hydrazine-aldehyde reaction produces a chromophore, which absorbs at 354 nm, allowing determination of the molarity of the CTT adducts on the BSA. Reaction conditions were adjusted so that the ratio of CTT peptide adducts to BSA was <0.5. This assures that most of the BSA molecules that have a CTT tail have only one CTT tail. Assays were performed with 50 nM CTTs or CTT-BSA constructs added to in vitro assays.

In vitro assays

We made a 10 μL flow chamber with double-stick tape (3M, St. Paul, MN), a slide, and a silanized coverslip (No. 1.5 Fisherbrand, Thermo Scientific). The coverslips were cleaned with acid and coated with 2% dimethyldichlorosilane (GE Healthcare, Wauwatosa, WI) to block the surface and prevent proteins from sticking to the surface of the coverslips. We first incubated 2% (w/v) MAB1864 tubulin antibody (YL1/2, Merck-Millipore, Billerica, MA) in katanin activity buffer (20 mM HEPES-HCl, pH 7.7, 10% glycerol, and 2 mM $MgCl_2$) for 5 min. Next, we added 5% (w/v) Pluronic F-127 in katanin activity buffer to additionally block the surface. Then fluorescent Taxol-stabilized microtubules were incubated in the chamber for 5 min. To remove excess microtubules, motility mix (20 mM HEPES-HCl, pH 7.7, 10% glycerol, 2 mM $MgCl_2$, 2 mM ATP, 0.025 mg/mL BSA, 0.05% F-127, 10 mM dithiothreitol, 15 mg/mL glucose, 0.15 mg/mL catalase, and 0.05 mg/mL glucose oxidase) was flowed into the chamber. The microtubules were imaged for 3 min to ensure that microtubules were present and bound to the surface. Next, motility mix with p60 (X. laevis p60 or GFP-labeled human p60) was flowed into the chamber during imaging. The protocols and buffers have been described in several previous studies by other groups and ourselves (9,18,22,29)

Imaging was performed using a Nikon Ti-E microscope with a homebuilt laser illumination system (30). Epifluorescence was used to image microtubules in the red or dark red channels, and total internal reflection fluorescence microscopy was used to image GFP-Hu-p60 in the green channel. Two-color imaging was performed by sequential exposure of different excitation wavelengths and paths using shuttering.

Loss of polymer and maximum GFP-Hu-p60 fluorescence quantification

The loss of microtubule polymer and the amount of GFP-Hu-p60 bound were quantified from fluorescence intensity measurements of the microtubule region over time using ImageJ (a specific illustration and example are shown in Fig. S1 in the Supporting Material). First, we used the line tool to draw a segmented line, 3 pixels wide, over the length of the micro-

tubule in the first frame, when the microtubule was complete. We used the macro measure stacks to measure the mean intensity of the same line over the microtubule for each frame of the movie. Next, the line was shifted to a region of background near the microtubule to measure the mean intensity of the background.

The mean intensity of each microtubule was divided by the mean intensity of the background nearby for each frame, thus giving a signal/noise relative intensity. We then subtracted 1 from each frame to remove the background. For microtubule fluorescence, the intensity was normalized for each data set such that the first frame in focus after p60 was added to the chamber was set to 1 (100%). This was performed to combine different microtubules that might have different mean intensities. The intensities were averaged over many microtubules for each frame. The standard deviation and standard error of the mean were calculated for each experimental parameter. This method is an accurate report of loss of polymer, because the microtubule is adhered to the surface along the length, and large segments of microtubule are not observed to dislodge. All data were plotted and fit as described in the text.

We also performed a similar analysis on data from the GFP-Hu-p60 channel. The mean intensity along the length of the microtubules was measured for the same region for each frame. The mean intensity was divided by the background mean GFP intensity to give a signal/noise ratio; we then subtracted 1 to remove the background. The resulting data were plotted as a function of time. The data from many microtubules in the same experimental parameters were averaged together. The maximal GFP fluorescence was determined from the averaged data. Fast frame-rate data were fit over time, and the association rate, oligomerization rate, and severing rate were determined by fitting the data, as described in the text below.

Analysis of the percentage of microtubules severed

Analysis of the percentage of microtubules severed was performed by counting the total number of microtubules in the movie and the number of microtubules that were severed at least once during the course of the movie.

RESULTS

Human p60 is as effective as *X. laevis* p60

Microtubule-severing assays have been performed previously to characterize severing enzymes (8-10,16,18,20,22,31-33). First, to show that our purified katanin is functioning, we performed microtubule-severing assays in vitro on Taxol-stabilized microtubules. We compared our new GFP-labeled human version of p60 (GFP-Hu-p60) to a previously characterized p60 from *X. laevis* (Xl-p60) (9,10). Qualitatively, we find that the severing activity of 50 nM GFP-Hu-p60 is as fast as that of 500 nM Xl-p60: a majority of the microtubules are severed by frames 3–7 in the series ~100–140 s, as seen in the representative time series (Fig. 1, *A* and *B*).

Similar to other methods of tracking microtubule severing, we used the average fluorescence intensity of the microtubule divided by the average background fluorescence intensity and normalized the initial intensity to 1 to plot the fraction of microtubule remaining in the microtubule region over time (see Materials and Methods and Fig. S1) (8-10,16,19,32,34). We do not use the number or
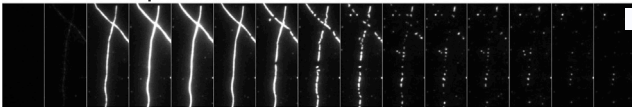
A X. laevis p60
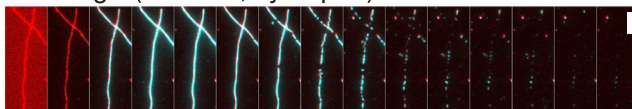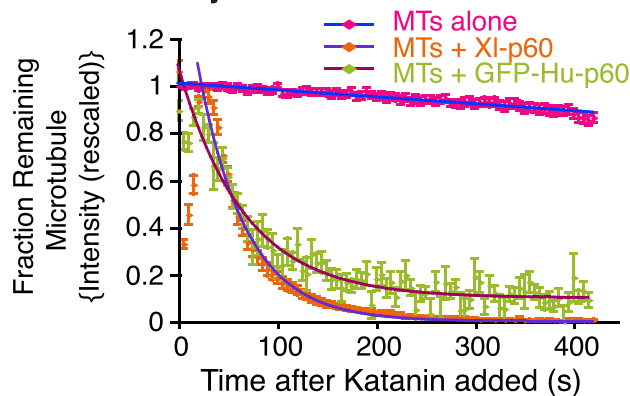### Dylight649-MTs
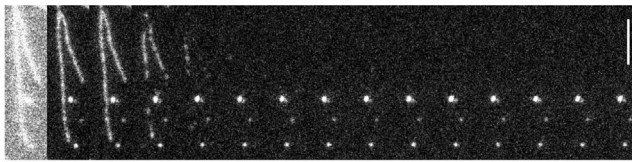
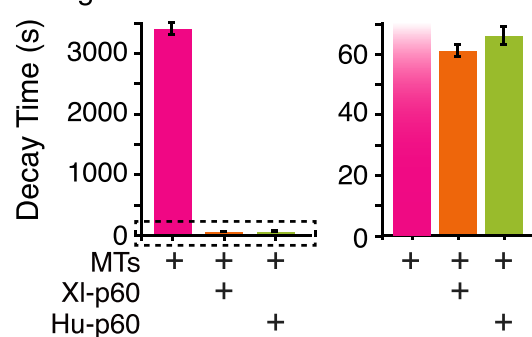## B Human p60
i. Dylight649-MTs
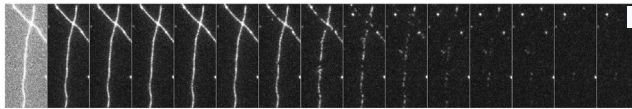
ii. GFP-Hu-p60

iii. Merge (red MTs, cyan p60)

(Δt = 10 s)

C Loss of Polymer over Time

D Characteristic Decay Times

i. Long times   ii. Short times

FIGURE 1   GFP human p60 is as effective as *X. laevis* p60. (*A*) Example time series of Dylight649 microtubules (MTs) being severed by *X. laevis* katanin-p60 (Xl-p60). The severing assays were 10 min long with a frame taken every 5 s. The times series depicts a frame every 10 s. The scale bar is 5 μm. By the end of the movie, the microtubules are completely destroyed. The first frame is bright and out of focus due to the enzyme being flowed

the length of microtubules over time, as has been done previously (31). We quantified the loss of polymer over time (Fig. 1 *C*). We found the rate of decay by fitting the data with an exponential decay function,

$$I(t) \;=\; I_0 \exp\!\left(-t/_{\tau}\right),\qquad(1)$$

where I represents the intensity as a function of time t, I_0 is the amplitude at time zero, and τ is the characteristic time constant for the decay (Fig. 1 *C*). This function assumed that the data will decay to 100% loss, but sometimes there were filaments or small remnants of filaments remaining. In this case, we fit the data to the following exponential decay with a vertical offset,

$$I(t) \;=\; I_0 \exp\!\left(-t/_{\tau}\right) + I_{\infty}.\qquad(2)$$

Here, I_{∞} is a vertical offset that takes into account that some of the filaments may remain, or that there might otherwise be a background fluorescence signal. The data from the *Xenopus* katanin, Xl-p60, was best fit by Eq. 1, with a characteristic decay rate of $\tau = 62 \pm 2$ s, with $R^2 = 0.95$ (Fig. 1 *D*; all fit parameters can be found in Table S1). The Human GFP katanin, GFP-Hu-p60, was best fit with equation 2 with a characteristic decay rate of $\tau = 66 \pm 3$ s, with $R^2 = 0.95$ (Fig. 1 *D* and Table S1).

When there is no katanin present, the data have a single, long characteristic decay time that is so long it appears linear. We can fit the data to a linear approximation for an exponential decay,

$$I(t) \;=\; I_0\!\left(1 - t/_{\tau}\right).\qquad(3)$$

Using this fit, we find the decay constant, τ, to be 3400 ± 100, with a goodness of fit of $R^2 = 0.93$ (Fig. 1 *D*; Table S1).

into the chamber. (*B*) Example two-color imaging time series of severing assays with GFP-Hu-p60. (*i*) Time series of Dylight649 microtubules in a severing assay with GFP-Hu-p60. Microtubules are completely destroyed by the end of the assay. The first frame is bright and out of focus due to the enzyme being flowed into the chamber. (*ii*) Time series of the same assay in (*i*) showing GFP-Hu-p60 binding along the microtubules. GFP-Hu-p60 was added during the first frame in the time series and, within two frames, is completely decorating the microtubules. (*iii*) A merge of (*i*) and (*ii*). Red is the Dylight649 microtubules and cyan is GFP-Hu-p60. The severing assays were 10 minutes long with a frame taken every 5 s. The times series depicts a frame every 10 s. The scale bars are 5 μm. (*C*) Quantification of fraction of microtubule polymer remaining over the course of severing assay for microtubules with Xl-p60 (*orange diamonds*, $N = 55$, fit to Eq. 2), microtubules with GFP-Hu-p60 (*green diamonds*, $N = 73$, fit to Eq. 1), and microtubules alone (*pink diamonds*, $N = 56$, fit to Eq. 3). Fit parameters are in Table S1. Error bars represent mean ± SE. (*D*) The characteristic decay times from the fits in (*C*). (*i*) Decay times depicted over the same, long scale. (*ii*) Decay times depicted over same short scale such that the data within the dashed rectangle of (*i*) are discernable.

Total time for katanin to complete severing is concentration dependent

We can also quantify the GFP fluorescence to uncover the binding and severing abilities of GFP-Hu-p60. To characterize the fast kinetics, we imaged continuously in the GFP-Hu-p60 channel (time between frames was 0.039 s). We quantified the GFP fluorescence intensity over time for each concentration of GFP-Hu-p60 (Fig. 2 A). Each time trace had a similar characteristic shape that includes three phases: 1) an early phase, where there was an exponential rise when GFP-Hu-p60 was binding to the microtubules (Fig. 2 B, i); 2) a constant phase with little change, which we term the pre-severing phase (35) (Fig. 2 B, ii); and 3) a late

time exponential decay, where the microtubules were being destroyed by the severing enzyme, resulting in loss of fluorescence (Fig. 2 B, iii). From these assays, we determined the time-dependent activities, including association time, pre-severing time, maximal GFP-Hu-p60 bound, and severing activity time (Fig. 2 A).

For each plot, we fit the initial exponential growth of binding (Fig. 2 B, i) to the equation

$$I(t) = A \exp(t/\tau_{bind}), \tag{4}$$

where A is the amplitude and τ_{bind} is the characteristic time for katanin binding (Fig. 2 B). The fit was performed on data
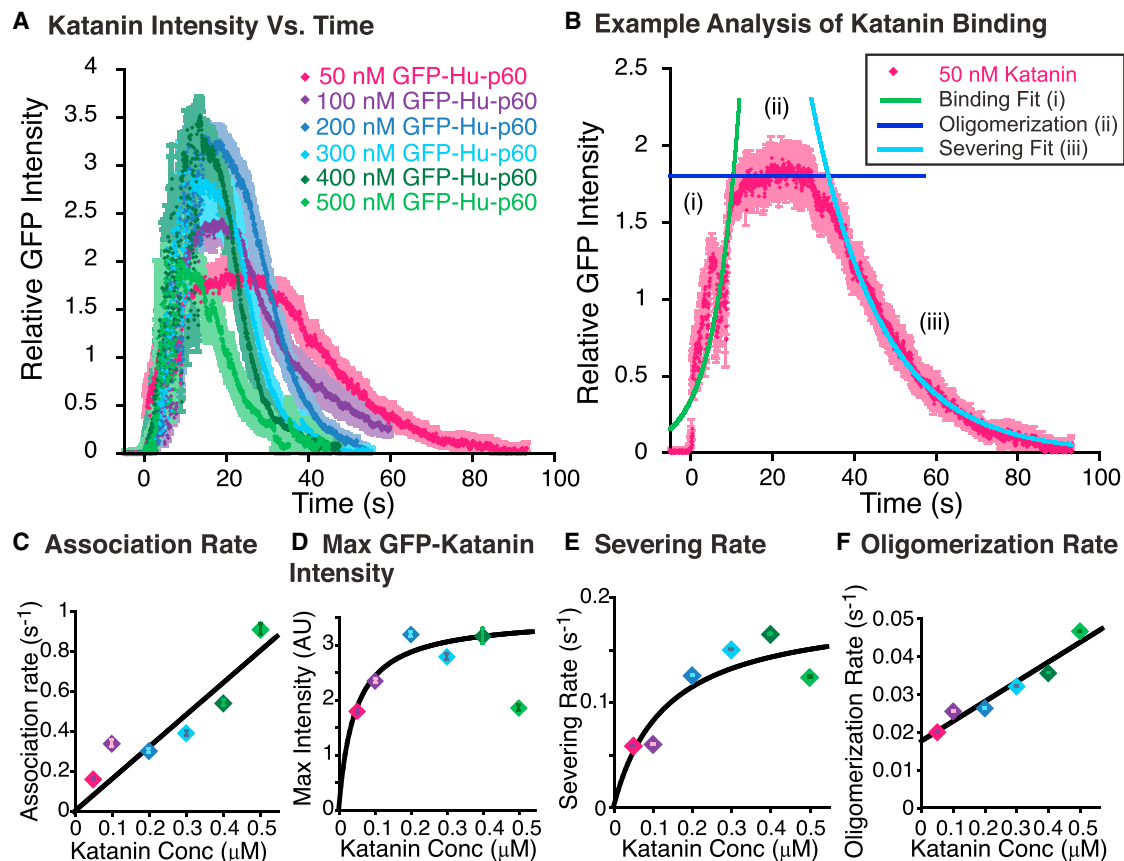

FIGURE 2 Fast katanin severing activities are concentration dependent. (A) Data of GFP-Hu-p60 binding and severing taken at 25.6 frames/s plotted over time after translating the data so that the binding occurs at $t = 0$ s. GFP-Hu-p60 concentrations were 50 nM (*pink diamonds, N = 13*), 100 nM (*purple diamonds, N = 51*), 200 nM (*dark blue diamonds, N = 48*), 300 nM (*light blue diamonds, N = 53*), 400 nM (*dark green diamonds, N = 25*), and 500 nM (*light green diamonds, N = 11*). Error bars (shown in paler versions of the marker colors) represent mean ± SE. (B) Example data set for 50 nM GFP-Hu-p60 shows the data (*pink diamonds*) has three distinct phases: (*i*) the exponential growth phase of GFP-Hu-p60 binding fit with Eq. 4 (*green line*), (*ii*) the pre-severing phase of oligomerization estimated as the average value (*dark blue line*), and (*iii*) the exponential decay phase where the katanin severs the microtubule fit with Eq. 5 (*light blue line*). (C) Characteristic binding rate from the fits to the initial binding phase plotted against katanin concentration. Error bars denote the uncertainty of the fit parameter. Data are fit to Eq. 6. (D) Plot of the maximum GFP intensity when GFP-Hu-p60 was bound in the pre-severing phase. Error bars represent mean ± SE. Data are fit to Eq. 7. (E) Plot of the characteristic severing rate from the fit to the severing phase plotted against the added katanin concentration. Error bars denote the uncertainty of the fit parameter. Data are fit to Eq. 8. (F) Plot of the oligomerization rate characterized by the pre-severing phase as a function of the added GFP-Hu-p60 concentration. Error bars represent propagated uncertainty from fit parameters τ_{bind} and t_0. Data are fit to Eq. 9. Fit parameters for all data sets can be found in Table S2. For (C)–(F), error bars are represented in front of the marker, but most were smaller than the marker size.

that had the longer-time data masked. The exact location of masking had little effect on the characteristic time for binding. Data for the initial exponential rise and pre-severing-phase data displayed significant intensity fluctuations due to the difficulty of imaging while pipetting severing enzyme into the flow chamber. These fluctuations are an artifact of the experimental method and are masked out for fitting the data.

We determined the average intensity over the pre-severing phase (Fig. 2 B, ii) by masking any increasing or decreasing data and measuring the average and standard deviation of the data points.

The exponential decay phase due to severing activity was fit to the exponential decay of the form

$$I(t) = \exp\left(\frac{t - t_0}{\tau_{sever}}\right), \quad (5)$$

where t_0 is the delay time to account for the time for phases 1 and 2 to complete. τ_{sever} is the characteristic time of the severing activity (Fig. 2 B). This equation is mathematically equivalent to Eq. 1, since exponential functions are self-similar. Fit parameters for all fits are given in Table S2.

From the data sets, fits, and fit parameters, we determine the association rate, pre-severing rate, maximal intensity of katanin binding, and the severing rate (Fig. 2, C–F). The association rate is the inverse of the characteristic association time determined from the fits to the exponential growth phase at short times (Eq. 4 and Fig. 2 B). The association rates reveal a linearly increasing dependence on GFP-Hu-p60 concentration (Fig. 2 C). We fit the data to a line of the form

$$r([p60]) = k_{on}[p60], \quad (6)$$

where the y-intercept is set to zero and the slope, k_{on}, gives the on-rate for katanin binding to microtubules. The best fit is given by $k_{on} = 0.0016 \pm 0.0002 \, (nM \, s)^{-1} = 1.6 \times 10^6 \, (M \, s)^{-1}$ (Fig. 2 C and Table S2). This is a reasonable association rate typical for proteins (36).

Next, we plotted the maximum average intensity during the pre-severing phase as a function of katanin concentration (Fig. 2 D). This measurement is similar to the total protein bound, as one might measure in an equilibrium-binding assay. We fit the data to a hyperbolic binding curve of the form:

$$I([p60]) = I_{max}\frac{[p60]}{K_D + [p60]}, \quad (7)$$

where I_{max} is the maximum intensity of binding and K_D is the equilibrium dissociation constant. The best fit to the data revealed $K_D = 45 \pm 20$ nM with a goodness of fit of $R^2 = 0.87$ (see Fig. 2 D and Table S2 for all fit parameters). Using the equilibrium dissociation constant from the fit to Fig. 2 D and the on rate from the fit to Fig. 2 C, we can es-

timate the off rate at steady state using $k_{off} = (K_D)(k_{on}) = 0.07 \pm 0.04 \, s^{-1}$.

The characteristic time to sever microtubules was determined by fitting Eq. 5 to the decay data at long time (Fig. 2 B, iii). The rate of severing was determined as the inverse of the characteristic time and plotted against the free katanin concentration (Fig. 2 E). Since this is the rate of an enzyme, we fit the data using canonical enzyme kinetic hyperbolic fit typified by Michaelis-Menten kinetics:

$$k([p60]) = k_{max}\frac{[p60]}{K_M + [p60]}, \quad (8)$$

where k_{max} is the maximum rate of enzyme activity (severing) and K_M is the characteristic concentration at which the rate is half the maximum rate. The maximum rate of severing was $0.19 \pm 0.04 \, s^{-1}$ and the K_M was 130 ± 80 nM, with a goodness of fit of $R^2 = 0.79$. Interestingly, the K_M is the same, within error, as the K_D for katanin. In enzyme activity, K_M is related to K_D such that $K_M = K_D + k_{enzyme}/k_{on}$, where k_{enzyme} is the rate of enzyme turn over (37). Considering that K_M is the same as K_D (within error), we conclude that the enzyme turnover rate is too fast for the resolution of our measurements.

If enzyme turnover is almost instantaneous in our experiments, it may be surprising that there is a pre-severing phase (Fig. 2 B, ii) between when the katanin binds (Fig. 2 B, i) and the severing begins (Fig. 2 B, iii). This phase may be the same as the pre-severing phase observed for spastin (35). We hypothesize that the pre-severing phase occurs because the katanin that binds is not capable of severing. Perhaps it is not yet hexamerized or bound to the correct location for activity. We estimate the pre-severing phase as the difference between the binding characteristic time, τ_{bind}, and the delay time for severing, t_0 (Eqs. 4 and 5). We call the inverse of this time the oligomerization rate, although there could be another process occurring to ready enzyme activity. Plotting the oligomerization rate against the GFP-Hu-p60 concentration, we have a linear increase and can fit the data with a line of the form

$$r([p60]) = r_0 + k_{olig}[p60], \quad (9)$$

where r_0 is the slowest rate at zero katanin concentration and k_{olig} is the hexamerization rate. The best fit for the oligomerization-rate data was $r_0 = 0.017 \pm 0.002 \, s^{-1}$ and $k_{olig} = 5.2 \pm 0.7 \times 10^4 \, (M \, s)^{-1}$, with a goodness of fit of $R^2 = 0.94$. The oligomerization rate is two orders of magnitude slower than the binding rate, causing the pre-severing phase to be obvious at low concentrations and less obvious at high concentrations.

Free tubulin inhibits katanin binding to microtubules

Results from previous studies have shown that katanin can be inhibited by the presence of dimeric tubulin adsorbed

to the glass of the chamber before performing a severing assay, although the effect was not quantified (6). More recent work with spastin has shown that severing can be inhibited by tubulin CTT peptides (24). We also observed that tubulin inhibited katanin severing in our own assays, and we sought to investigate the mechanism of such inhibition.

Using our severing assays, we added free tubulin to the chamber with GFP-Hu-p60 or Xl-p60 katanin to quantify the inhibitory effects of dimers. Surprisingly small concentrations of tubulin dimers (50 nM) showed significant reduction of severing. Any concentration of free tubulin >500 nM completely abolished severing (Fig. 3, A and B). We quantified the loss of polymer by monitoring individual microtubule loss of fluorescence, as above. We fit the data to exponential decays or linear approximations to decays depending on the best fit (Eqs. 1–3 and Table S3). The same pattern of severing inhibition held true for the unlabeled *X. laevis* construct (Fig. S2), suggesting that free tubulin is a universal inhibitor of katanin severing.

Examination of the GFP-Hu-p60 shows that the inhibition of severing is due to a loss of katanin binding to microtubules (Fig. 3 A). We quantified the maximal fluorescence of GFP-Hu-p60 binding and found a significant decrease in katanin binding with increasing concentrations of additional tubulin (Fig. 3, A and C). We fit the data to a modified Hill equation to capture the inhibition kinetics of the form

$$c[\text{tub}] = c_0 \left(\frac{1}{1 + \left([\text{tub}] / K_{\text{D,app}} \right)^n} \right), \qquad (10)$$

where c_0 is the amplitude at zero additional tubulin concentration [tub], $K_{\text{D,app}}$ is an apparent equilibrium concentration of tubulin for inhibition, and n is a Hill coefficient. The apparent equilibrium constant is 80 ± 10 nM, and the Hill coefficient is 0.8 ± 0.05 with a goodness of fit of $R^2 = 0.998$. That the Hill coefficient is <1 is interesting and indicates that it is a bit harder for the second katanin to bind once the first is bound. This makes sense for a multicomponent oligomerization and competition scheme.

We found that the characteristic concentration for tubulin to inhibit katanin severing is only 80 nM. For comparison, the critical concentration of tubulin polymerization is ~1.8 μM, and the critical concentration for polymerization in the presence of Taxol is 0.08 μM (38,39). This explains why Taxol-stabilized microtubules that have little free tubulin in the background are easily severed. On the other hand, dynamic microtubules will be much more difficult to sever, because free dimers in the background will inhibit severing. Interestingly, the concentration of free tubulin in a cell is thought to be between 5 and 25 μM, depending on the cell type (40,41).

A Time series of Severing Inhibition with Tubulin Addition

All scale bars 5 µm
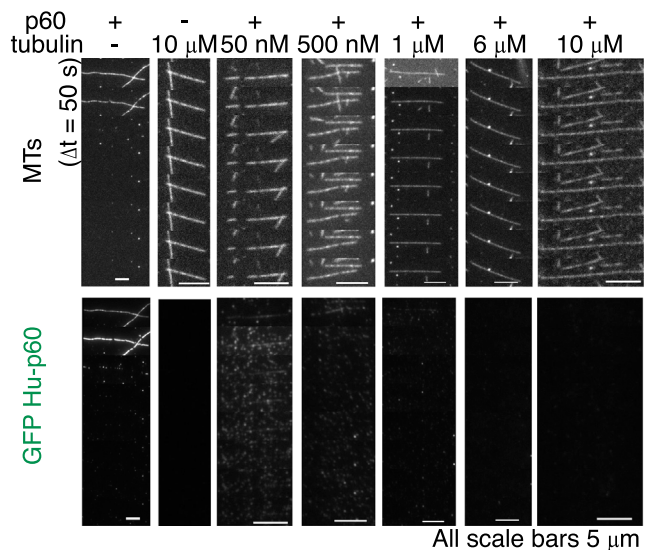
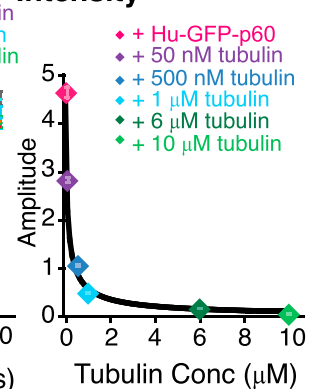## B Loss of Polymer over Time
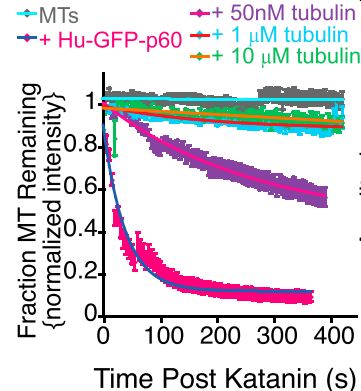
C Max GFP-Katanin Intensity

FIGURE 3 Katanin's severing activity is inhibited by free tubulin. (*A*) Example time series of severing by GFP-Hu-p60 with free tubulin at concentrations from 0–10 μM. Severing assays were performed for 10 min with an exposure every 5 s. Time between displayed frames is 50 s. The scale bars are 5 μm. (*B*) Plot of loss of polymer of microtubule as a function of time for tubulin concentrations of 0 nM (pink diamonds), 50 nM (*purple diamonds*), 1 μM (*light blue diamonds*), 10 μM (*green diamonds*), and no GFP-Hu-p60 control (*gray diamonds*). (*C*) Plot of the maximum GFP-Hu-p60 fluorescence. The data are best fit by a modified Hill function in Eq. 10. For all data displayed, the number of microtubules analyzed is: 0 nM (*pink diamonds*, N = 83), 50 nM (*purple diamonds*, N = 73), 500 nM (*dark blue diamonds*, N = 42), 1 μM (*light blue diamonds*, N = 42), 6 μM (*dark green diamonds*, N = 44), and 10 μM free tubulin (*light green diamonds*, N = 46). All fit equation, parameters, and goodness of fits are given in Table S3.

Katanin has a higher affinity for free tubulin than microtubules in severing assays

We have shown that dimers can inhibit binding of katanin when the tubulin and katanin are added simultaneously (Fig. 3). In the experiments presented above, the katanin could be binding to tubulin before being added to the assay

because they are premixed before insertion into the chamber. To test whether tubulin can compete with microtubule polymer for binding, we created a flow-in experiment to directly observe whether katanin bound to the microtubule can be competed off by excess dimers. The GFP-Hu-p60 was bound to microtubules in the presence of ATPγS, a slowly hydrolyzable analog of ATP, allowing katanin to bind to microtubules but not sever. Then we added 0 nM (buffer only), 50 nM, 500 nM, 1 μM, 6 μM, and 10 μM of free tubulin to the chamber and monitored the GFP-Hu-p60 fluorescence on the microtubules over time (Fig. 4 A).

We quantified the GFP-Hu-p60 fluorescence over time and fit the loss of GFP fluorescence to an exponential decay equation (Eq. 2, Fig. 4 B, and Table S4). It was qualitatively obvious that as more tubulin was added, more katanin was dissociated from the microtubule (Fig. 4, A and B). The characteristic decay times were a result of dissociation of GFP-Hu-p60 from the microtubules due to competition between the microtubule filament and free tubulin.

Using the characteristic decay times, we found the decay rates, which correspond to the apparent rate of katanin loss in the presence of tubulin. We plotted the dissociation rate against the concentration of tubulin added (Fig. 4 C, i). We fit the data to a line of equation

$$r([\text{tub}]) = r_0 + k_{\text{replace,tub}}[\text{tub}], \qquad (11)$$

where r is the observed rate of loss of katanin, [tub] is the added tubulin concentration, $k_{\text{replace,tub}}$ is the tubulin-dependent rate, and r_0 is the intercept with the y axis when the tubulin concentration is zero (Fig. 4 C; Table S4). Similar to Eq. 9, we have a nonzero intercept, implying that even at zero tubulin, we would measure a small rate of loss. The best fit parameters were $r_0 = 0.018 \pm 0.002$ s^{-1}, $k_{\text{replace,tub}} = 1.2 \pm 0.4 \times 10^3$ (M s)$^{-1}$, with goodness of fit $R^2 = 0.77$. The rate of tubulin loss in the absence of tubulin, r_0, should be equivalent to the dissociation rate, k_{off}. We previously used the fits from Fig. 2, C and D, to estimate k_{off} and found $k_{\text{off}} = 0.07 \pm 0.04$ s^{-1}. Using this new observation, we can estimate $k_{\text{off}} \sim r_0 = 0.018 \pm 0.002$ s^{-1}. These two separate estimates are the same order of magnitude, although they are not exactly the same as one another. Considering the propagated uncertainties from each measurement, it is perhaps not surprising that they are not exactly the same.

For each of our exponential decay fits, there was a long-time asymptote to which the data decayed, I_∞ (Eq. 2 and Fig. 4 B), that was nonzero. This represents the fraction of GFP-Hu-p60 that remained bound after addition of the tubulin. We plotted the remaining katanin intensity as a function of the concentration of added tubulin (Fig. 4 C, ii). We fit the data to Eq. 10, since inhibition is caused by competition between tubulin dimers and polymer. The apparent equilibrium constant is 40 ± 30 nM, and the Hill coefficient is 0.4 ± 0.3, with a goodness of fit of
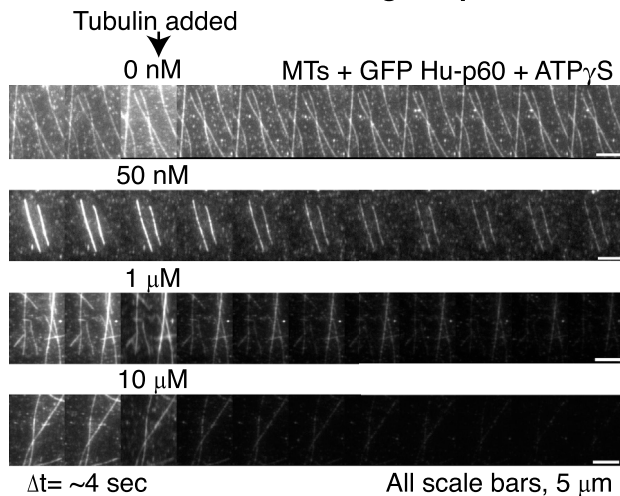
$R^2 = 0.97$. These data are not as well fit as Fig. 3 C, but the fit parameters are the same order of magnitude and within uncertainty. Although it is perhaps obvious, these data show that competition for katanin by free tubulin dimers drives the inhibition of severing activity we observe. Interestingly, when the concentration of katanin is high relative to the background tubulin concentration, the time to sever is only ~50 s (Fig. 3 B, 0 free tubulin data). These data imply that as long as the katanin concentration is much higher than the free tubulin concentration, severing will proceed.

It is perhaps surprising that free tubulin could compete and cause the dissociation of katanin even in the ATP-bound state of the enzyme. Previous results with AAA+ enzymes imply that the ATP-bound state, mimicked by the slowly hydrolyzable analog ATPγS, should be the tightly bound state (42). Yet we observed ready dissociation of katanin even in the presence of ATPγS. There are two possible explanations for this. Either the ATP state is not high affinity or the katanin is not fully hexamerized and has lower affinity in the monomeric or small oligomeric form. We cannot discern the differences here, but these are interesting questions to probe in future experiments.
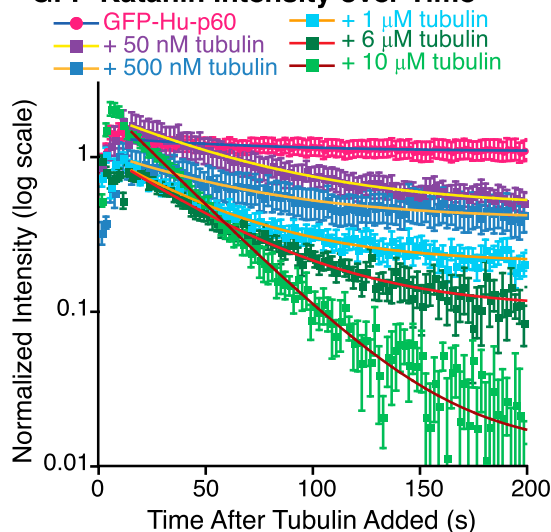
Katanin recognizes sequence of C-terminal tail of free tubulin

Katanin-p60 has been proposed to have two possible microtubule-binding sites: the microtubule interacting and trafficking site at the N-terminus of p60 (amino acids 55–180), and the pore loop region in the AAA domain (amino acids 197–488) that binds to the tubulin CTT (20,31,33). Next we wanted to distinguish whether katanin was binding to dimer due to recognizing and binding to the specific shape or folded structure of the tubulin or whether katanin was recognizing a specific sequence of tubulin, most likely through the tubulin CTTs. To address this question, we unfolded free tubulin using acid denaturation and brought the concentration back to neutral pH to use in the assay. Since tubulin requires a chaperone to fold, the neutralized protein should be improperly folded or unfolded. To specifically probe whether the CTT was needed, we also made denatured free tubulin with the CTTs cleaved off by treating microtubules with the protease subtilisin before denaturing the microtubules. We performed the same experiment, where we added GFP-Hu-p60 with free tubulin at 50 nM, denatured tubulin at 50 nM, or subtilisin-treated denatured tubulin at 50 nM. We monitored both the microtubule signal to inspect severing and polymer loss and the GFP-channel to quantify katanin binding (Fig. 5 A). As was clear from the time series (Fig. 5 A), both free tubulin and denatured tubulin were able to inhibit katanin severing and binding. However, the subtilisin-treated, denatured tubulin did not inhibit severing but had quantifiable effects on GFP-Hu-p60 binding.

A Free Tubulin Flow Through Experiments

Tubulin added

0 nM   MTs + GFP Hu-p60 + ATPγS

50 nM

1 μM

10 μM

Δt= ~4 sec   All scale bars, 5 μm

B GFP-Katanin Intensity over Time

Legend:
- GFP-Hu-p60 (pink circles)
- + 50 nM tubulin (yellow/purple squares)
- + 500 nM tubulin (orange/blue squares)
- + 1 μM tubulin (light blue squares)
- + 6 μM tubulin (dark green squares)
- + 10 μM tubulin (red/green squares)

Y-axis: Normalized Intensity (log scale)
X-axis: Time After Tubulin Added (s)

C Characteristic Decay Rate and Intensities

Legend:
- GFP-Hu-p60 (pink circles)
- + 50 nM tubulin (purple squares)
- + 500 nM tubulin (dark blue squares)
- + 1 μM tubulin (light blue squares)
- + 6 μM tubulin (dark green squares)
- + 10 μM tubulin (light green squares)

i. Characteristic Decay Rate
Y-axis: Characteristic Decay Rate (s⁻¹)
X-axis: Tubulin Conc (μM)

ii. Final Intensity
Y-axis: Final Intensity (normalized)
X-axis: Tubulin Conc (μM)
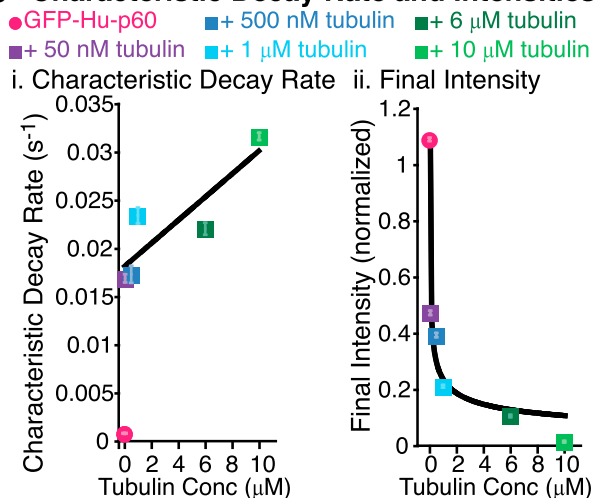
FIGURE 4 Katanin has a higher affinity for free tubulin than microtubules. (*A*) Example time series of unbinding of GFP-Hu-p60 via free tubulin at concentrations of 0 nM, 50 nM, 1 μM, and 10 μM free tubulin.

We quantified the fraction of microtubules remaining over time and fit each data set to the exponential decays (Fig. 5 *B* and Table S5). Both the free-tubulin and denatured-tubulin experiments lose very little of the polymer (Fig. 5, *A* and *B*). Interestingly, when tubulin was treated with subtilisin to remove CTTs and denatured, the severing activity was almost completely recovered to the same level as in control experiments without free tubulin (Fig. 5 *C*). Further, the fraction of total polymer lost was similar for katanin alone and in the presence of subtilisin-treated tubulin (Fig. 5 *D*). Also interestingly, denatured tubulin was more effective at inhibiting severing than folded tubulin when comparing the rates of polymer loss and the overall loss of polymer (Fig. 5, *C* and *D*).
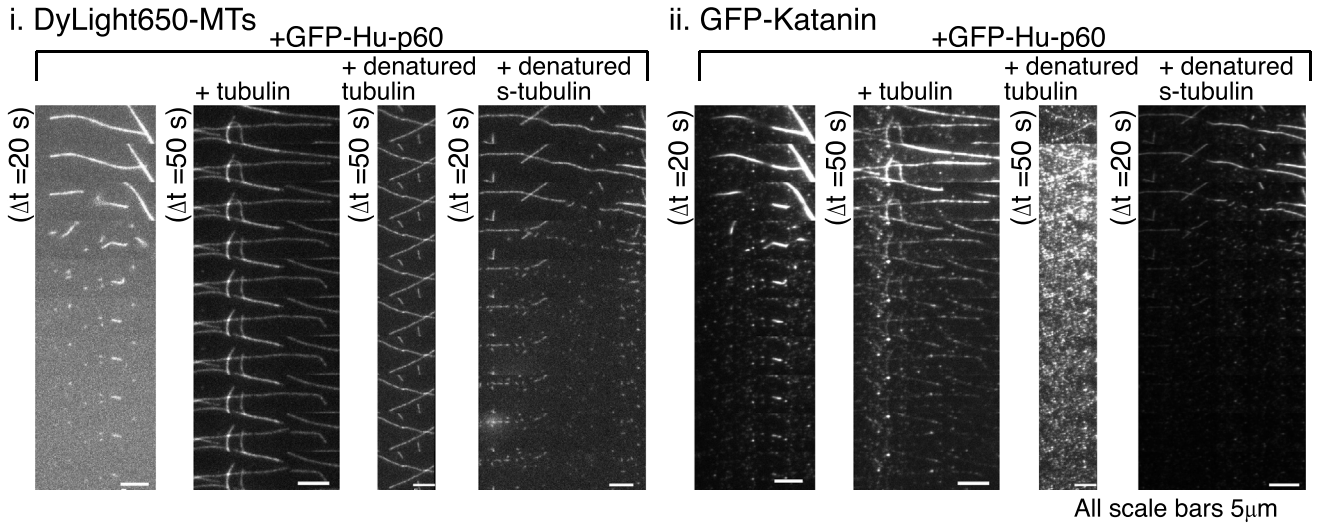
Quantification of the maximum GFP fluorescence demonstrates that the lack of severing activity was due to a lack of katanin binding to the microtubules (Fig. 5, *A* and *F*) and was directly proportional to the overall loss of polymer (Fig. 5, *B* and *D*). Combining these results, we infer that katanin does not recognize the shape of the folded tubulin. Rather, the binding of katanin to the CTT is required for effective inhibition of binding and severing.

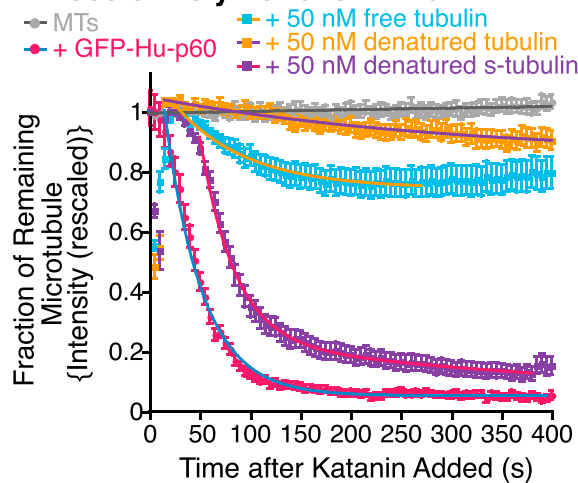## Katanin has a higher affinity for the β- than for the α-tubulin CTT

We have demonstrated that the CTTs of tubulin are essential for effective inhibition of severing activity (Fig. 5). Each tubulin dimer has two CTTs, one α and one β. We sought to investigate which CTT is a better inhibitor of katanin and thus a better competitor for the katanin binding. To address these questions, we created peptide sequences of human α- and β-tubulin CTTs. Using click chemistry (43),

FIGURE 5 Katanin is effectively inhibited by denatured tubulin but not subtilisin-treated denatured tubulin. (A) Example time series of severing via GFP-Hu-p60 with tubulin, denatured tubulin, or denatured subtilisin-treated tubulin (denatured s-tubulin). The severing assays were 10 min with a frame taken every 5 s. (i) Time series of the dylight649-MTs signal for each of the conditions. (ii) Time series of GFP-Hu-p60 signal for each of the conditions. The time series show frames every 20 s or 50 s as stated. The scale bars are 5 μm. (B) Quantification of the fraction of the microtubule remaining over time with fits for each of the following conditions: microtubules alone (gray circles), microtubules with GFP-Hu-p60 alone (pink circles), microtubules with 50 nM GFP-Hu-p60 and 50 nM folded tubulin (light blue squares), microtubules with 50 nM GFP-Hu-p60 and 50 nM denatured tubulin (orange squares), and microtubules

(legend continued on next page)

we covalently bound the CTT constructs to BSA protein to make CTT-BSA chimeras (see Materials and Methods and Sheldon et al. (28)). A background concentration of BSA protein already exists in our assays, so the addition of BSA is controlled.

We observed distinct differences in the ability to sever depending on whether the CTT constructs were α or β. Specifically, very few severing events occurred when the β tails were present (Fig. 6 A). When the α tails were present, we saw severing events and some loss of polymer from the ends of filaments, suggesting that the α-tubulin tails could inhibit, but were not as effective as β-tubulin CTTs (Fig. 6 A). We quantified the fraction of remaining polymer over time and fit the data to exponential decays (Fig. 6 B and Table S6). In the presence of all CTT-BSA chimeras, the loss of microtubule polymer occurred with a relatively short characteristic decay time (Fig. 6 C), but there was a significant amount of remaining polymer (Fig. 6, B and D). The data indicated that β tails were better inhibitors of severing than α tails (Fig. 6, A and D).

We quantified the fraction of microtubules that displayed at least one severing event. The trend was identical to the total loss of polymer and confirms that the β-tubulin CTT inhibits better than the α-tubulin CTT (Fig. 6 D). We also quantified binding of the GFP-Hu-p60 to microtubules (Fig. 6 F). Interestingly, we found that the maximum GFP fluorescence for katanin binding is not exactly mimicking the trends for loss of polymer (Fig. 6 D) or percentage of filaments severed (Fig. 6 E). In particular, the β-CTT allowed as much binding to microtubules as free tubulin but inhibited better than the full dimers. This result implies that the β tails may inhibit severing through a slightly altered mechanism, but our current data cannot distinguish the exact differences. Future work with this construct at varying concentrations may shed light on the mechanism of β-tubulin CTT inhibition of katanin.

We repeated these measurements with CTT polypeptides without the BSA, and found similar amounts of inhibition with the same concentration of free CTTs (50 nM) (Fig. S3). This is perhaps surprising, since we anticipated that CTTs without BSA would be less potent inhibitors than the CTTs covalently attached to BSA. Our results imply that the CTTs alone are capable of inhibiting katanin severing without the need to block the pore using a large globular protein. The concentration was 10-fold lower than that needed to block spastin activity (24), implying

that this regulation scheme is more potent for katanin than spastin.

Katanin has lower affinity for detyrosinated α-tubulin

Using the same scheme to make CTT-BSA polypeptide chimeras, we were able to make a version of the α-CTT with the final tyrosine missing. Such detyrosinated tubulin is typically a marker of reduced microtubule dynamics in cells (44). We added 50 nM of the deytosinated α-CTT-BSA chimeras to severing assays and found that the microtubules were still severed (Fig. 6 A), but the overall rate of severing and overall loss of polymer were reduced compared to controls with GFP-Hu-p60 alone (Fig. 6, B–D). The total polymer lost, percentage of filaments severed, and amount of GFP-Hu-p60 binding were directly proportional, implying that the inhibition of severing was again due to a reduction in katanin binding in the presence of detyrosinated α-tubulin CTT-BSA chimeras. In comparison to the α- and β-tubulin CTT-BSA chimeras, detyrosinated α-tubulin was the least effective inhibitor of all the CTT peptides (Fig. 6). Similar results were found using CTT tails alone (Fig. S3).

DISCUSSION

We used quantitative methods to analyze a human version of the enzymatic portion of the microtubule-severing enzyme katanin, p60. We analyzed both the severing activity and the binding activity and found that binding is tight and directly proportional to severing activity, although we did observe a concentration-dependent pre-severing lag time, which could be due to oligomerization or another event (Fig. 2). Further, we show that severing can be inhibited by free tubulin, denatured tubulin, and the CTTs, and that this inhibition is entirely due to the competition between microtubules and tubulin dimers for the binding of katanin.

We find that it takes significantly more Xl-p60 (500 nM) than GFP-Hu-p60 (50 nM) to sever microtubules to the same qualitative activity levels. In our previously published work (22), we showed that *Drosophila* katanin p60 (Dm-p60) acts even slower than Xl-p60 or GFP-Hu-p60. During this slow activity, Dm-p60 depolymerized microtubules (22). In our current study, the severing activity of GFP-Hu-p60 is too quick to monitor depolymerization. Future work where GFP-Hu-p60 is slowed through various means would be

with 50 nM GFP-Hu-p60 and 50 nM denatured subtilisin-treated tubulin (*purple squares*). Error bars represent mean ± SE. (*C*) Characteristic decay times from the fit equations from the data in (*B*). Error bars represent the uncertainty of the fit parameters. (*D*) Amount of microtubule polymer lost from the fit equations to the data in (*B*). Error bars represent the uncertainty of the fit parameters. (*E*) Quantification of the fraction of microtubules that displayed at least one resolvable severing event over the experiment. (E) Plot of the maximum GFP-Hu-p60 fluorescence for each condition. For all data displayed, the number of microtubules analyzed is: microtubules along (*gray*, N = 25), GFP-Hu-p60 alone (*pink*, N = 50), GFP-Hu-p60 with folded tubulin (*light blue*, N = 57), GFP-Hu-p60 with denatured tubulin (*orange*, N = 42), and GFP-Hu-p60 with subtilisin-treated denatured tubulin (*purple*, N = 46). All fit equations, parameters, and goodness of fits are given in Table S5.

A Timeseries

i. DyLight650-MTs   +GFP-Hu-p60

+ tubulin   +β-CTTs   +α-CTTs   +αΔY-CTTs

ii. GFP-Katanin   +GFP-Hu-p60

+ tubulin   +β-CTTs   +α-CTTs   +αΔY-CTTs

All scale bars 5 μm

B Loss of Polymer over Time

- MTs
- + GFP-Hu-p60
- + 50 nM free tubulin
- + 50 nM β-CTTs
- + 50 nM α-CTTs
- + 50 nM αΔY-CTTs

C Characteristic Decay Times

D Total Loss of Polymer

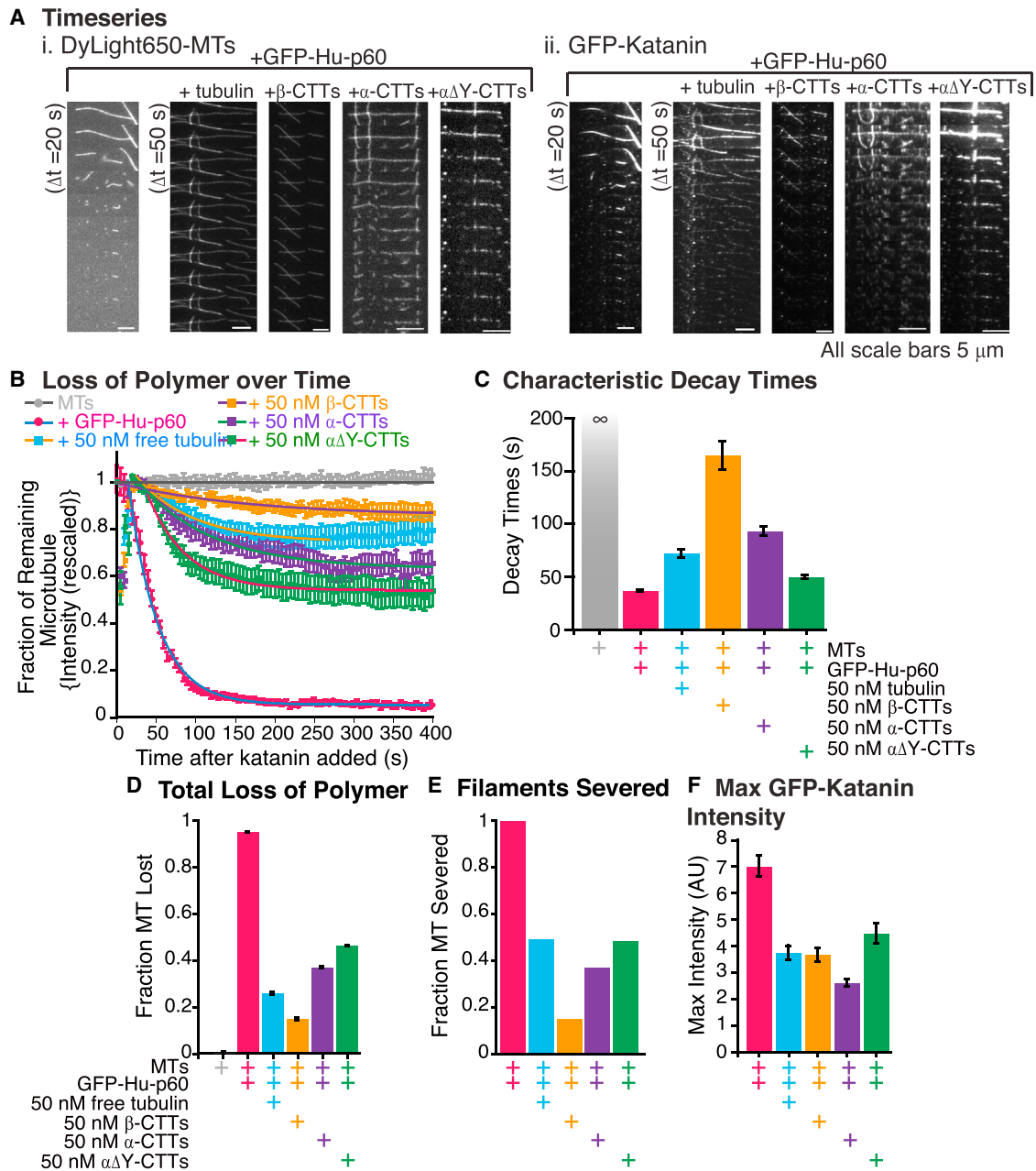## E Filaments Severed

F Max GFP-Katanin Intensity

FIGURE 6   Katanin is most effectively inhibited by β-tubulin c-terminal tails. (A) Example time series of severing via GFP-Hu-p60 in the presence of CTT-BSA chimeras. (i) Time series of dylight649-MTs signal in severing assays for microtubules with katanin, microtubules with katanin and β-CTT-BSA, α-CTT-BSA, and detyrosinated α-CTT. (ii) Same time series viewed in the GFP-Hu-p60 channel. The severing assays were 10 min with a frame taken every 5 s. The time series show frames every 20 s or 50 s as stated. The scale bars are 5 μm. (B) Plot of the fraction of the microtubule remaining over time with fit to data for each of the following conditions: microtubules only (*gray circles*), microtubules with 50 nM GFP-Hu-p60 (*pink circles*), microtubules with 50 nM GFP-Hu-p60 and 50 nM tubulin (*light blue squares*), microtubules with 50 nM GFP-katanin and 50 nM β-CTT-BSA (orange squares), microtubules with 50 nM GFP-Hu-p60 and 50 nM α-CTT-BSA (*purple squares*), and microtubules with 50 nM GFP-Hu-p60 and 50 nM detyrosinated α-CTT-BSA (*green squares*). Error bars represent mean ± SE. (C) Characteristic decay times from the fits to the loss of polymer data in (B). Error bars represent the uncertainty of the fit parameters. (D) Amount of microtubule polymer lost from the fit equations to the data in (B). Error bars represent the uncertainty of the fit parameters. (E) Quantification of the fraction of microtubules that displayed at least one resolvable severing event over the experiment. (F) Plot of the maximum GFP-Hu-p60 fluorescence for each condition. For all data displayed, the number of microtubules analyzed is: microtubules alone (*gray*, $N = 25$), GFP-Hu-p60 alone (*pink*, $N = 50$), GFP-Hu-p60 with free tubulin (*light blue*, $N = 57$), GFP-Hu-p60 with β-CTTs (*orange*, $N = 40$), GFP-Hu-p60 with α-CTTs (*purple*, $N = 59$), and GFP-Hu-p60 with detyrosinated CTTs (*green*, $N = 33$). All fit equations, parameters, and goodness of fits are given in Table S6.

informative for determining whether GFP-Hu-p60 can depolymerize, as well as sever, microtubules.

We found that severing is inhibited by tubulin introduced simultaneously with katanin (Fig. 3). Further, tubulin can remove katanin already bound to microtubules (Fig. 4). Tubulin dimers seem to be working as an irreversible inhibitor under the conditions in our assay. Once the katanin binds the dimer, it can no longer bind to microtubules; thus, it effectively decreases the concentration of available, active katanin in the experiment. Interestingly, one of the products of severing is tubulin dimers, the inhibitor. Thus, the severing reaction has a negative feedback mechanism that should stop severing after a certain point. Prior work has shown that high concentrations of microtubules can result in a lower ATPase rate for katanin (3,4,19). This may be due to poisoning by released dimers.

Our results demonstrate that katanin is effectively inhibited by free tubulin in vitro at tubulin concentrations well below the cellular concentration, estimated to be ~2 mg/mL (18 μM) (40,41). Even if half of the tubulin is in the form of microtubules, there is still 10 μM of free tubulin available in cells. We observed that katanin's severing activity was inhibited at low dimer concentration, 50 nM (Fig. 3). Our assays typically used 50–200 nM katanin, so the lowest concentration was effectively 1:1 tubulin/katanin. This is a much lower concentration range than previously probed. The p60-p80 complex was shown to bind to microtubules better than tubulin dimers when there was a 1:5 ratio of p60-p80 to tubulin (5). Spastin severing was inhibited by a 10-fold molar excess of tubulin tails (25). In addition, Roll-Mecak and Vale found that 0.5 mM β-CTT peptide significantly inhibited spastin severing activity (24), yet they did not quantify the inhibition as we have done here. Based on our quantification, one would expect to need at least as much katanin as free tubulin to cause any type of severing or microtubule regulation in a live cell. This could be achieved by a relatively high concentration of katanin or a relatively low concentration of free tubulin. In the cell, severing activity could be regulated by the relative concentrations of katanin to free tubulin in solution.

In our prior work, we showed that Drosophila katanin was highly enriched at the cell cortex where it acted locally to keep microtubules short in S2 cells (18). Although we could not quantify the concentration of katanin in cells, our results presented here imply that there was as much katanin as free tubulin. Overall, our work suggests that the ratio of katanin to free tubulin is an effective means to regulate katanin's activity in cells. If the cell needs to locally destroy microtubules, localizing high concentrations of katanin greater than the concentration of tubulin dimers would allow such activity.

In addition to relative concentration, other cellular factors could regulate the activity of katanin. Future work could test whether p80 could enhance p60 severing activity and over-come dimer inhibition. It was previously shown that in microtubule pelleting assays with 200 μg/mL microtubules, 200 μg/mL free tubulin, and 40 μg/mL p60/p80, katanin still pelleted with the microtubule polymers and not with the soluble tubulin (5). This result suggests that katanin p60/p80 has a higher affinity for microtubules than for dimers. Subsequent work showed that the p80 subunit enhances the affinity of p60 for microtubules in vitro (8). In vivo, a fully functional set of p60 and p80 subunits is required for efficient targeting and severing activity (8). This evidence provides one plausible explanation for how katanin can sever microtubules in vivo despite displaying a high affinity for tubulin dimers in vitro. Future in vitro experiments with both p60 and p80 should be performed to determine whether the katanin heterodimer (p60/p80) can overcome the inhibition by the tubulin dimers by increasing the binding of p60 to the microtubule lattice.

Another possible mechanism for avoiding inhibition of katanin in vivo is other MAPs binding and sequestering tubulin. There are several examples of MAPs that are known to bind tubulin dimers. Many, but not all, of these MAPs are involved in stabilizing microtubules or contribute to growing microtubules by recruiting tubulin dimers to the growing end of the microtubule. Tau-protein is known to bind to soluble tubulin dimers, and mutant tau-proteins bind with even higher affinity (45). Proteins from the CLASP and chTOG families are also known to bind free tubulin (46). Further, CLASP can bind to the microtubule polymer and the tubulin at the same time to recruit dimers to the growing ends of microtubules (47). Microtubule destabilizers also bind tubulin dimers. Stathmin, a microtubule catastrophe factor, binds to tubulin dimers (48) and is likely to sequester tubulin (49). E-like, a novel protein similar to the chaperone cofactor E, causes depolymerization of microtubules by sequestering and even degrading the free tubulin pool (50). Taken together with our results, we hypothesize that future in vitro experiments of severing in the presence of stabilizing MAPs will incongruously show enhanced severing and microtubule polymer loss.

Our results directly point to the ratio of katanin to free tubulin as a switch for katanin severing activity. Some cellular locations of known katanin activity have lower free tubulin concentration. For instance, katanin is highly expressed in embryonic tissue, where there is a lot of cell proliferation and lower tubulin concentration (51). Katanin p80 and p60 are also highly expressed in the central nervous system, and in cultured neuronal cells, p80 is enriched predominately in the cell body, and p60 is found at higher levels in axons (51). In axons, the microtubules tend to be more stable and less dynamic than in other cells, implying that there is less free tubulin. Katanin would therefore not be affected nearly as much by free tubulin and in fact may be the source of tubulin dimers to enable axon growth.

Our results reveal that the ability to impede severing is based on the ability of the katanin to bind to the inhibitor

better than microtubule polymer. Since the inhibitor is the tubulin dimer itself, our results could address the ability of katanin to bind to different types of tubulin. More credence is given to this idea by the fact that tubulin dimers missing the CTT cannot inhibit severing. Previous work has shown that katanin and spastin are both unable to sever subtilisin-treated microtubules (5,20,23). This implies that the inhibition is driven by the katanin binding to the CTTs, and not to a secondary site, such as the microtubule interacting and trafficking domain.

Our microtubules and tubulin dimers are derived from porcine brains with a mix of α and β isotypes and numerous posttranslational modifications. To examine the effects of α- and β-tubulin CTTs separately, as well as the effect of α-tubulin detyrosination, we created peptides of CTTs covalently linked to BSA and tested their inhibitory activities individually. All were able to inhibit to some degree. This is consistent with prior results reported for spastin, where CTT peptides were able to bind spastin (25) and could inhibit spastin severing (24). Our results demonstrate that the sequence of the CTT alters the ability to inhibit (Fig. 6). Interestingly, our work reveals distinct differences between katanin and spastin. First, previous studies showed that spastin did not bind to tubulin dimers, only tails alone or microtubules (25). Further, prior studies showed that only relatively high concentrations (500 μM) of β-tubulin CTT peptide could inhibit spastin severing, but the same concentration of α CTTs could not (24). In contrast, we have clearly demonstrated that katanin can bind to tubulin CTTs specifically and tightly both with a globular domain (BSA) and without (Figs. 6 and S3). Further, we used low concentrations of CTT-BSA or CTTs (50 nM) and found potent inhibition of both binding of katanin to the microtubule substrate and severing. Such differences are likely the result of altered differences in katanin and spastin binding and targeting in cells. One reason katanin and spastin may be regulated differently is that spastin may not need to be turned off, because it is not free in the cytosol but rather is associated with membranous vesicles (23,52).

We showed that detyrosination of the α-tubulin CTT reduces the inhibitory effect of the CTTs (Fig. 6), which could imply that detyrosinated tubulin is a less effective substrate for katanin binding. Our results imply that katanin is distinct from spastin, which bound to tyrosinated and detyrosinated tubulin CTTs equally well (25). We find that katanin can bind to detyrosinated tubulin, but binds much better to tyrosinated α-tubulin CTTs. If this result holds for katanin binding to tubulin in the microtubule lattice, it would imply that katanin would target tyrosinated tubulin over detyrosinated tubulin. Downregulation of katanin on detyrosinated (Glu) microtubules would result in enhanced stability of this population of microtubules. Indeed, it is known that detyrosinated microtubules are less dynamic and slower to incorporate new tubulin than tyrosinated microtubules (44). Another microtubule destabilizer, MCAK, prefers to depolymerize tyrosinated microtubules, but when overexpressed, it will depolymerize detyrosinated tubulin (53).

There are many other types of posttranslational modifications of tubulin that can regulate how MAPs bind to microtubules (54,55). Most modifications occur on the CTTs, including detyrosination, polyglutamylation, and polyglycylation. Acetylation of tubulin occurs on the lumen surface. Each type of posttranslational modification has been shown to affect the activity of some severing enzymes both in vivo (15,56,57) and in vitro (5,20,23,25). Given this evidence, it is likely that posttranslational modifications of tubulin play a role in regulating katanin. Whether this is direct regulation by serving as targets for enhanced severing, indirect regulation by inhibition of katanin, or regulation by influencing the binding of other MAPs that may inhibit or enhance katanin severing activity is still unclear. Future experiments examining other tubulin CTT sequences and posttranslational modifications would be very interesting. Perhaps most intriguing would be to examine the effects of polyglutamylation or polyglycosylation, which have been shown to be potent regulators of spastin (56).

Our results lead us to conclude that katanin's severing activity is concentration dependent. It is inhibited by free tubulin dimers and specifically and differentially by the CTTs of tubulin. Future studies with increasingly complex systems including p80, stabilizing MAPs, and other posttranslationally modified CTTs need to be performed to address how katanin is regulated, and such studies will shed new light on how it works in vivo.

SUPPORTING MATERIAL

Three figures and six tables are available at http://www.biophysj.org/biophysj/supplemental/S0006-3495(15)01168-6.

AUTHOR CONTRIBUTIONS

ACKNOWLEDGMENTS

REFERENCES

1. Desai, A., and T. J. Mitchison. 1997. Microtubule polymerization dynamics. *Annu. Rev. Cell Dev. Biol.* 13:83–117.

2. Frickey, T., and A. N. Lupas. 2004. Phylogenetic analysis of AAA proteins. *J. Struct. Biol.* 146:2–10.

3. Hartman, J. J., J. Mahr, …, F. J. McNally. 1998. Katanin, a microtubule-severing protein, is a novel AAA ATPase that targets to the centrosome using a WD40-containing subunit. *Cell.* 93:277–287.

4. Hartman, J. J., and R. D. Vale. 1999. Microtubule disassembly by ATP-dependent oligomerization of the AAA enzyme katanin. *Science.* 286:782–785.

5. McNally, F. J., and R. D. Vale. 1993. Identification of katanin, an ATPase that severs and disassembles stable microtubules. *Cell.* 75:419–429.

6. Vale, R. D. 1991. Severing of stable microtubules by a mitotically activated protein in *Xenopus* egg extracts. *Cell.* 64:827–839.

7. Soga, K., A. Yamaguchi, …, T. Hoson. 2010. 1-aminocyclopropane-1-carboxylic acid (ACC)-induced reorientation of cortical microtubules is accompanied by a transient increase in the transcript levels of γ-tubulin complex and katanin genes in azuki bean epicotyls. *J. Plant Physiol.* 167:1165–1171.

8. McNally, K. P., O. A. Bazirgan, and F. J. McNally. 2000. Two domains of p80 katanin regulate microtubule severing and spindle pole targeting by p60 katanin. *J. Cell Sci.* 113:1623–1633.

9. Loughlin, R., J. D. Wilbur, …, R. Heald. 2011. Katanin contributes to interspecies spindle length scaling in *Xenopus. Cell.* 147:1397–1407.

10. Whitehead, E., R. Heald, and J. D. Wilbur. 2013. N-terminal phosphorylation of p60 katanin directly regulates microtubule severing. *J. Mol. Biol.* 425:214–221.

11. Ahmad, F. J., W. Yu, …, P. W. Baas. 1999. An essential role for katanin in severing microtubules in the neuron. *J. Cell Biol.* 145:305–315.

12. Murata, T., S. Sonobe, …, M. Hasebe. 2005. Microtubule-dependent microtubule nucleation based on recruitment of γ-tubulin in higher plants. *Nat. Cell Biol.* 7:961–968.

13. Nakamura, M., and T. Hashimoto. 2009. A mutation in the Arabidopsis γ-tubulin-containing complex causes helical growth and abnormal microtubule branching. *J. Cell Sci.* 122:2208–2217.

14. Dymek, E. E., P. A. Lefebvre, and E. F. Smith. 2004. PF15p is the chlamydomonas homologue of the katanin p80 subunit and is required for assembly of flagellar central microtubules. *Eukaryot. Cell.* 3:870–879.

15. Sharma, N., J. Bryant, …, J. Gaertig. 2007. Katanin regulates dynamics of microtubules and biogenesis of motile cilia. *J. Cell Biol.* 178:1065–1079.

16. McNally, K., E. Berg, …, F. J. McNally. 2014. Katanin maintains meiotic metaphase chromosome alignment and spindle structure in vivo and has multiple effects on microtubules in vitro. *Mol. Biol. Cell.* 25:1037–1049.

17. McNally, K., A. Audhya, …, F. J. McNally. 2006. Katanin controls mitotic and meiotic spindle length. *J. Cell Biol.* 175:881–891.

18. Zhang, D., K. D. Grode, …, D. J. Sharp. 2011. *Drosophila* katanin is a microtubule depolymerase that regulates cortical-microtubule plus-end interactions and cell migration. *Nat. Cell Biol.* 13:361–370.

19. Stoppin-Mellet, V., J. Gaillard, and M. Vantard. 2002. Functional evidence for in vitro microtubule severing by the plant katanin homologue. *Biochem. J.* 365:337–342.

20. Eckert, T., D. T. Le, …, G. Woehlke. 2012. Spastin's microtubule-binding properties and comparison to katanin. *PLoS One.* 7:e50161.

21. Davis, L. J., D. J. Odde, …, S. P. Gross. 2002. The importance of lattice defects in katanin-mediated microtubule severing in vitro. *Biophys. J.* 82:2916–2927.

22. Díaz-Valencia, J. D., M. M. Morelli, …, J. L. Ross. 2011. *Drosophila* katanin-60 depolymerizes and severs at microtubule defects. *Biophys. J.* 100:2440–2449.

23. Roll-Mecak, A., and R. D. Vale. 2005. The *Drosophila* homologue of the hereditary spastic paraplegia protein, spastin, severs and disassembles microtubules. *Curr. Biol.* 15:650–655.

24. Roll-Mecak, A., and R. D. Vale. 2008. Structural basis of microtubule severing by the hereditary spastic paraplegia protein spastin. *Nature.* 451:363–367.

25. White, S. R., K. J. Evans, …, B. Lauring. 2007. Recognition of C-terminal amino acids in tubulin by pore loops in Spastin is important for microtubule severing. *J. Cell Biol.* 176:995–1005.

26. Le, D. T., T. Eckert, and G. Woehlke. 2013. Computer simulation of assembly and co-operativity of hexameric AAA ATPases. *PLoS One.* 8:e67815.

27. Peloquin, J., Y. Komarova, and G. Borisy. 2005. Conjugation of fluorophores to tubulin. *Nat. Methods.* 2:299–303.

28. Sheldon, K. L., P. A. Gurnev, …, D. L. Sackett. 2015. Tubulin tail sequences and post-translational modifications regulate closure of mitochondrial voltage-dependent anion channel (VDAC). *J. Biol. Chem.* 290:26784–26789.

29. Diaz-Valencia, J. D., M. Bailey, and J. L. Ross. 2013. Purification and biophysical analysis of microtubule-severing enzymes in vitro. *Methods Cell Biol.* 115:191–213.

30. Ross, J. L., and R. Dixit. 2010. Multiple color single molecule TIRF imaging and tracking of MAPs and motors. *Methods Cell Biol.* 95:521–542.

31. McNally, F. J., and S. Thomas. 1998. Katanin is responsible for the M-phase microtubule-severing activity in *Xenopus* eggs. *Mol. Biol. Cell.* 9:1847–1861.

32. Buster, D., K. McNally, and F. J. McNally. 2002. Katanin inhibition prevents the redistribution of γ-tubulin at mitosis. *J. Cell Sci.* 115:1083–1092.

33. Johjima, A., K. Noi, …, T. Ogura. 2015. Microtubule severing by katanin p60 AAA+ ATPase requires the C-terminal acidic tails of both α- and β-tubulins and basic amino acid residues in the AAA+ ring pore. *J. Biol. Chem.* 290:11762–11770.

34. McNally, K. P., D. Buster, and F. J. McNally. 2002. Katanin-mediated microtubule severing can be regulated by multiple mechanisms. *Cell Motil. Cytoskeleton.* 53:337–349.

35. Eckert, T., S. Link, …, G. Woehlke. 2012. Subunit Interactions and cooperativity in the microtubule-severing AAA ATPase spastin. *J. Biol. Chem.* 287:26278–26290.

36. Pollard, T. D. 2010. A guide to simple and informative binding assays. *Mol. Biol. Cell.* 21:4061–4067.

37. Howard, J. 2001. Mechanics of motor proteins and the cytoskeleton. 2001. Sunderland, MA. Sinauer.

38. Schiff, P. B., J. Fant, and S. B. Horwitz. 1979. Promotion of microtubule assembly in vitro by taxol. *Nature.* 277:665–667.

39. Shelanski, M. L., F. Gaskin, and C. R. Cantor. 1973. Microtubule assembly in the absence of added nucleotides. *Proc. Natl. Acad. Sci. USA.* 70:765–768.

40. Hiller, G., and K. Weber. 1978. Radioimmunoassay for tubulin: a quantitative comparison of the tubulin content of different established tissue culture cells and tissues. *Cell.* 14:795–804.

41. Gard, D. L., and M. W. Kirschner. 1987. Microtubule assembly in cytoplasmic extracts of *Xenopus* oocytes and eggs. *J. Cell Biol.* 105:2191–2201.

42. Vale, R. D. 2000. AAA proteins. Lords of the ring. *J. Cell Biol.* 150:F13–F19.

43. Banerjee, A., T. D. Panosian, …, S. Bane. 2010. Site-specific orthogonal labeling of the carboxy terminus of α-tubulin. *ACS Chem. Biol.* 5:777–785.

44. Kreis, T. E. 1987. Microtubules containing detyrosinated tubulin are less dynamic. *EMBO J.* 6:2597–2606.

45. Elbaum-Garfinkle, S., G. Cobb, …, E. Rhoades. 2014. Tau mutants bind tubulin heterodimers with enhanced affinity. *Proc. Natl. Acad. Sci. USA.* 111:6311–6316.

46. Al-Bassam, J., M. van Breugel, …, A. Hyman. 2006. Stu2p binds tubulin and undergoes an open-to-closed conformational change. *J. Cell Biol.* 172:1009–1022.

47. Al-Bassam, J., H. Kim, …, F. Chang. 2010. CLASP promotes microtubule rescue by recruiting tubulin dimers to the microtubule. *Dev. Cell.* 19:245–258.

48. Belmont, L. D., and T. J. Mitchison. 1996. Identification of a protein that interacts with tubulin dimers and increases the catastrophe rate of microtubules. *Cell.* 84:623–631.

49. Howell, B., N. Larsson, …, L. Cassimeris. 1999. Dissociation of the tubulin-sequestering and microtubule catastrophe-promoting activities of oncoprotein 18/stathmin. *Mol. Biol. Cell.* 10:105–118.

50. Bartolini, F., G. Tian, …, N. J. Cowan. 2005. Identification of a novel tubulin-destabilizing protein related to the chaperone cofactor E. *J. Cell Sci.* 118:1197–1207.

51. Yu, W., J. M. Solowska, …, P. W. Baas. 2005. Regulation of microtubule severing by katanin subunits during neuronal development. *J. Neurosci.* 25:5573–5583.

52. Evans, K. J., E. R. Gomes, …, B. P. Lauring. 2005. Linking axonal degeneration to microtubule remodeling by Spastin-mediated microtubule severing. *J. Cell Biol.* 168:599–606.

53. Peris, L., M. Wagenbach, …, A. Andrieux. 2009. Motor-dependent microtubule disassembly driven by tubulin tyrosination. *J. Cell Biol.* 185:1159–1166.

54. Roll-Mecak, A. 2015. Intrinsically disordered tubulin tails: complex tuners of microtubule functions? *Semin. Cell Dev. Biol.* 37:11–19.

55. Janke, C. 2014. The tubulin code: molecular components, readout mechanisms, and functions. *J. Cell Biol.* 206:461–472.

56. Lacroix, B., J. van Dijk, …, C. Janke. 2010. Tubulin polyglutamylation stimulates spastin-mediated microtubule severing. *J. Cell Biol.* 189:945–954.

57. Sudo, H., and P. W. Baas. 2010. Acetylation of microtubules influences their sensitivity to severing by katanin in neurons and fibroblasts. *J. Neurosci.* 30:7215–7226.